Journal of Information Display, vol. 3, no. 3, 2002

Silicon-based 0.69-inch AMOEL Microdisplay with Integrated Driver Circuits

Young Sun Na and Oh Kyong Kwon*

Abstract

Silicon-based 0.69-inch AMOEL microdisplay with integrated driver and timing controller circuits for microdisplay applications has been developed using 0.35 μm 1-poly 4-metal standard CMOS process with 5 V CMOS devices and CMP (Chemical Mechanical Polishing) technology. To reduce the large data programming time consumed in a conventional current programming pixel circuit technique and to achieve uniform display, de-amplifying current mirror pixel circuit and the current-mode data driver circuit with threshold roltage compensation are proposed. The proposed current-mode data driver circuit is inherently immune to the ground-bouncing effect. The Monte-Carlo simulation results show that the proposed current-mode data driver circuit has channel-to-channel non-uniformity of less than ±0.6 LSB under ±70 mV threshold voltage variaions for both NMOS and PMOS transistors, which gives very good display uniformity.

Keywords : AMOEL microdisplay, de-amplifying current mirror, current mode data driver circuit

1. Introduction

In the past several years OEL (Organic Electro-Luminescent) display has drawn great interest, because of its many attractive properties such as fast response time, large viewing angle, and simple device structure, which are suited for the flat panel display. Recent several reports [1-6] have dealt with AM (Active Matrix) driving technologies of OEL display using TFT (Thin Film Transistor) technology. One of the reasons for using the TFT technology is to make larger-size displays. On the other hand, the successful demonstration of the silicon-based AMOEL microdisplay for head-wearable application [8] has shown that the OEL display is also suitable for the small-size display. In the various trials for making AMOEL display, irrespective of whether it is formed on the TFT substrate or silicon substrate, the enhancement of display uniformity has been a major concern.

Among the several efforts to improve the display uniformity of AMOEL display, the current programmable pixel circuit technique [3-5] is very effective because it compensates for both the threshold voltage and the mobility variations of each pixel circuit. But this circuit technique has severe problem of very long pixel data programming time due to the relative large capacitance of data line compared to the very low-level pixel current. To overcome this problem, the de-amplifying current mirror pixel circuit [6,7] was proposed and was first realized in the 13.0-inch TFT AMOEL display [6]. But, the TFT technology has severe mismatch problem. That is, even the nearest two transistors have different threshold voltages and mobilities in TFT technology. Such a mismatch problem in the TFT technology is dramatically reduced in Single crystalline silicon technology [7]. And in case of small-size silicon-based AMOEL microdisplay, the large pixel data programming time also exists, which will be

Manuscript received June 26, 2002; accepted for publication August 30, 2002.
This work was supported by LG Electronics Inc. In Korea.
*Member, KIDS.
Corresponding Author : Young Sun Na
Divisin of Electrical and Computer Engineering, Hanyang University 17 Hangdang-dong, Seongdong-ku, Seoul 133-791, Korea.
E-mail : okwon7@chollian.net **Tel** : +2 2297-0139 **Fax** : +2 2297-7701

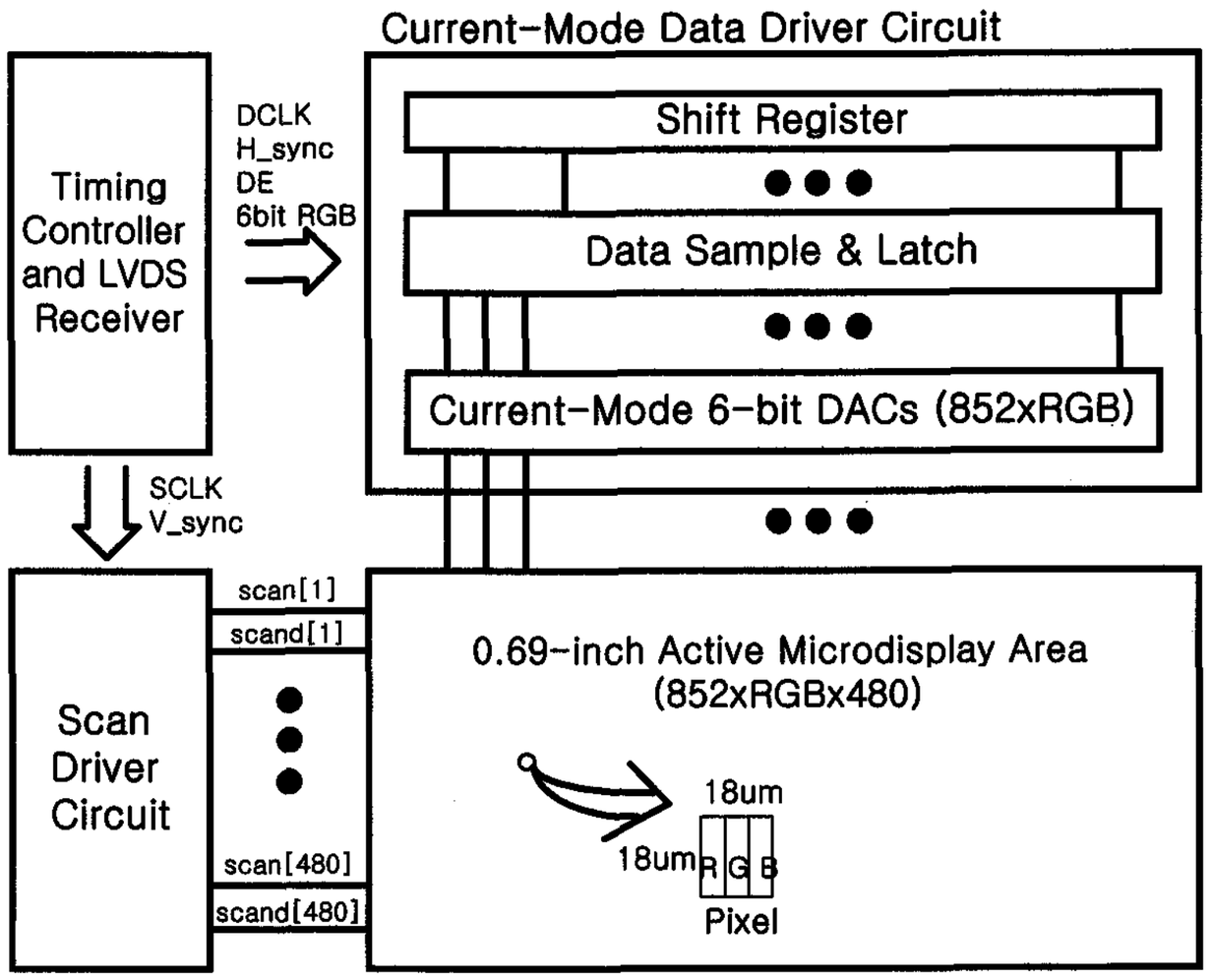

Fig. 1. The block diagram of silicon-based AMOEL microdisplay system.

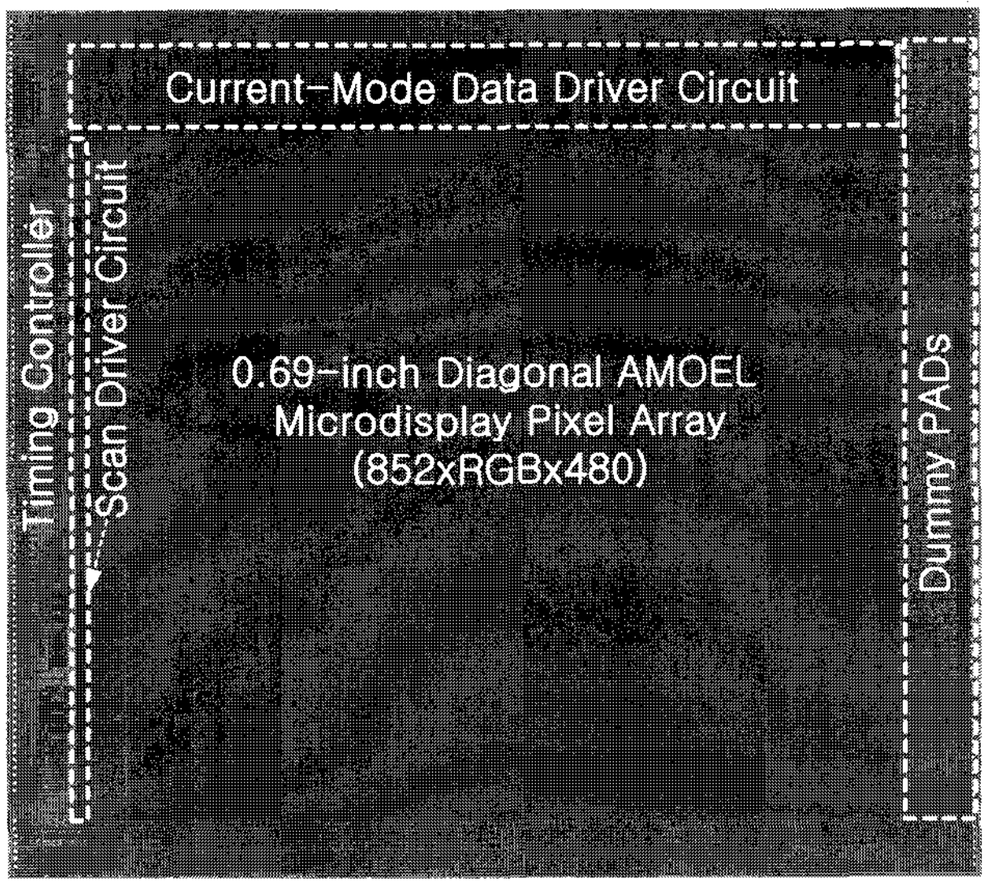

Fig. 2. The chip photograph of silicon-based 0.69-inch AMOEL microdisplay system.

discussed in Section 2. So, this de-amplifying current mirror pixel circuit technique is also very useful for the silicon-based AMOEL microdisplay.

To operate a AMOEL display having current programmable pixel circuits, the current-mode data driver circuit is needed. As it is the data driver circuit that programs the current programmable pixel circuit, the display uniformity of AMOEL display gradually begins depend on the current-mode data driver circuit and not on the current programmable pixel circuit itself. So, the current-mode data driver circuit should have uniform channel-to-channel outputs. But the current-mode data driver circuit normally has a current-mode DAC (Digital-to-Analog Converter) for each output channels, which are spread wide in layout. So, unavoidable threshold voltage mismatches exist among transistors in

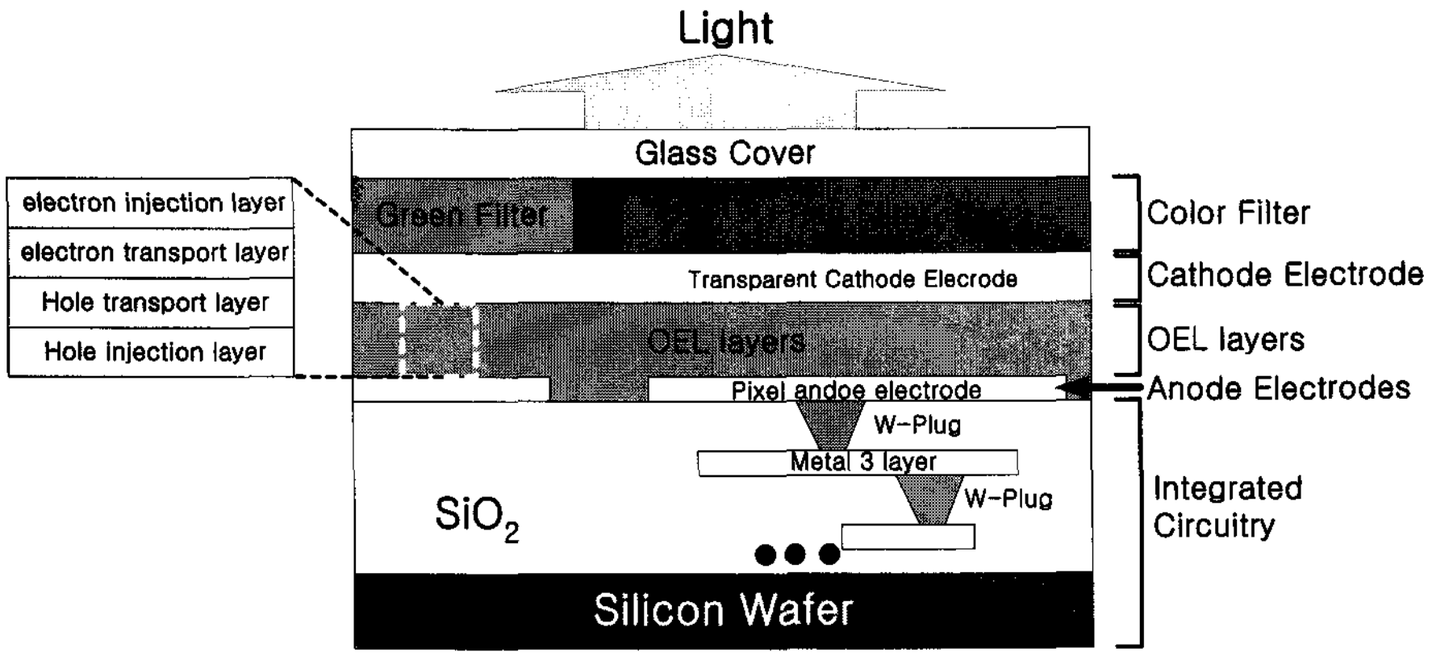

Fig. 3. The cross-sectional diagram of active microdisplay area in Fig. 1.

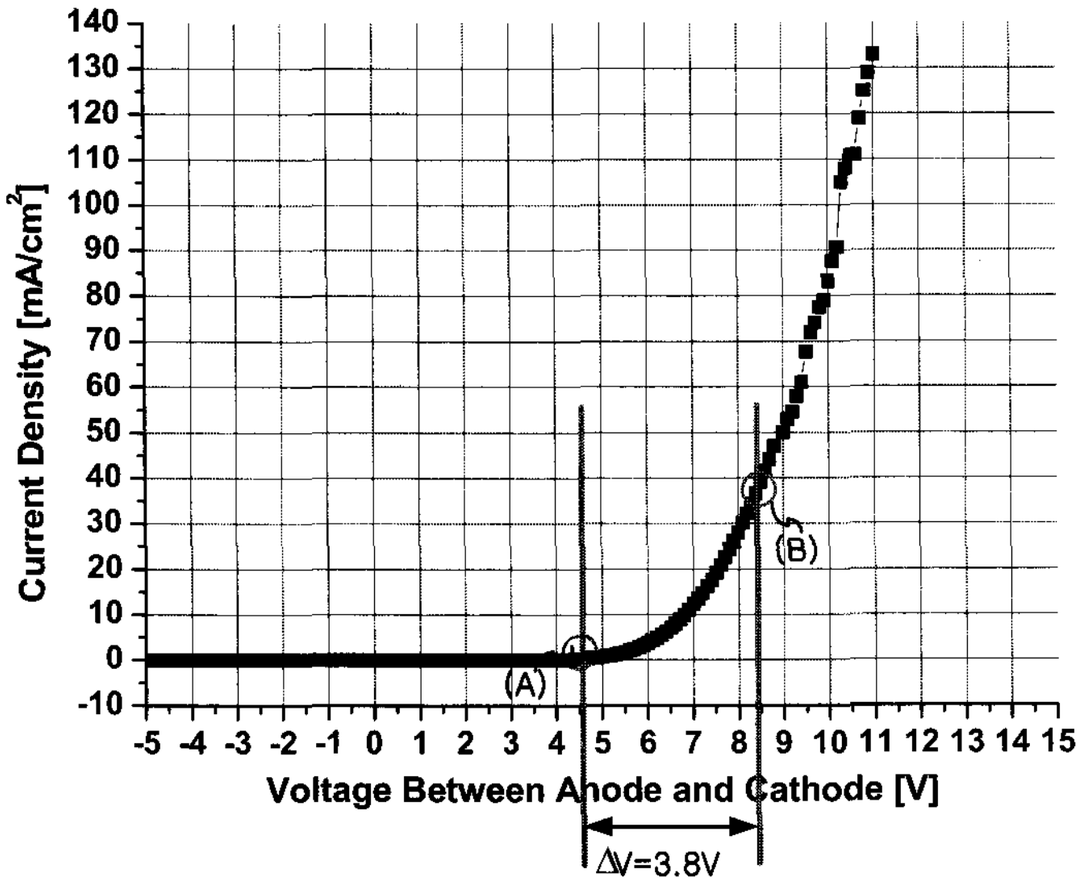

Fig. 4. The I-V characteristic of the OEL pixel.

current-mode DACs. To obtain uniform current outputs, a current source with threshold voltage compensation is necessary. S.Y. Chin and C. Y. Wu [9] proposed a current source circuit with useful threshold voltage compensation scheme for the 10-bit DAC, where the output current is proportional to the threshold voltage difference between neighbouring two transistors that have the same widths and lengths. Using this threshold voltage compensation concept, the binary-weighted 6-bit current-mode DAC for the current mode data driver circuit has been proposed. The proposed current mode data driver circuit has also been proven to have immunity to the ground-line voltage fluctuations (ground-bouncing) that will be described in Section 3.

In Section 2, the silicon-based AMOEL microdisplay system and de-amplifying current-mirror pixel circuit are described. The linear relationship of the sampled pixel currents versus input programming data currents is also shown. In Section 3, the current-mode data driver circuit with threshold voltage compensation is discussed. The effect of threshold voltage compensation for the uniform display is shown by Monte Carlo simulation. And, lastly conclusions are drawn in Section 4.

2. Silicon-based AMOEL Microdisplay with De-amplifying Current Mirror Pixel Circuit

Fig. 1 shows the block diagram of silicon-based AMOEL microdisplay system. It consists of 0.69-inch active microdisplay area with the resolution of 852 (×RGB)×480, current-mode data driver circuit, scan driver circuit, and timing controller. The functions of each circuit blocks in Fig. 1 are as follows. In the current-mode data driver circuit, the 6-bit RGB digital video data are sampled and converted into currents through binary-weighted current-mode 6-bit DACs. And the currents are programmed into each pixel in the active microdisplay area. The scan driver circuit generates V_{scan} and V_{scand} waveforms. The V_{scand} waveform is generated from V_{scan} waveform with some timing delay to reduce sampling errors, which will be described later. The timing controller generates clock signals (DCLK, SCLK) and several control signals. All the circuit blocks including active microdisplay area have been integrated on the same chip. Fig. 2 shows the photograph of the realized AMOELD backbone chip using a 0.35 μm 1-poly 4-metal standard CMOS process with CMP technology.

Fig. 3 shows the cross-sectional diagram of active microdisplay area in Fig. 1. On the single crystalline silicon wafer, pixel circuits are integrated. The CMP process on each metal layer should be used to avoid uneven OEL material processing in the active microdisplay area in Fig. 1. After anode electrode patterning, white OEL layers (hole injection layer, hole transport layer, electron transport layer, and electron injection layer to the top-ward direction) are formed. Thereafter, transparent cathode electrode layer and colour conversion layer are formed successively. The light is seen from the top.

Fig. 4 shows the I-V characteristic of the OEL pixel. Considering the net pixel area of 74.25 μm^2 (=4.5×16.5 μm^2), to obtain 150 cd/m^2 at the front side of the microdisplay panel, the pixel current is 27 nA at the anode to cathode voltage of 8.4 V because the pixel current density at that voltage is 36.36 mA/cm^2, as shown (B) in Fig. 4. And the turn on voltage of the OEL is about 4.6 V, as shown (A) in Fig.4. The anode to cathode voltage difference for points (A) and (B) in Fig. 4 is about 3.8 V. This is the reason why the 4.5 V power supply voltage for the integrated driver circuit using 5 V CMOS devices and the –4.6 V supply voltage for the transparent common cathode electrode are used. Because the peak pixel current level is 27 nA at the luminance of 150 cd/m^2 at the front side of the microdisplay panel, the black level pixel current of 270 pA is chosen to achieve a 100:1 contrast ratio. And the 6-bit RGB video data interface achieves 420 pA for 1-LSB grey levels. If the conventional current programmable pixel circuit [3-5], as shown in Fig. 5, is chosen, the pixel data programming time T_P can be calculated using the following equation [6]:

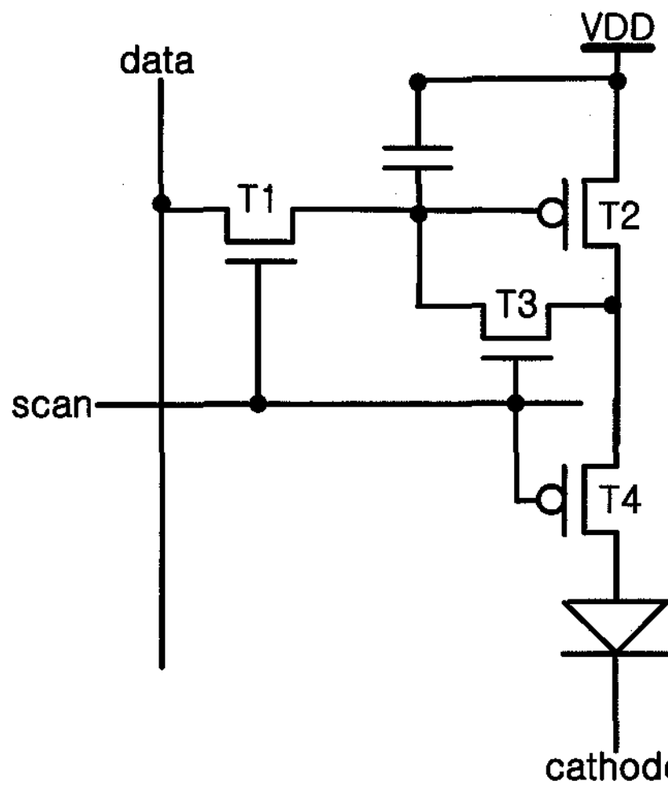

Fig. 5. A conventional current programmable pixel circuit.

$$T_p = \frac{C \bullet V_{max}}{2\sqrt{I_{data} \bullet I_{max}}} \bullet \ln\left(1 + \frac{2}{\sqrt{1 + \Delta I / I_{data}} - 1}\right) \qquad (1)$$

where C is the data line capacitance, I_{max} is the maximum current that corresponds to the peak luminance, V_{max} is the voltage swing of the data line. In the calculation, the sequence of writing small I_{data} after writing a large current is assumed to simplify calculation without considering the initial condition. For example, let us assume the following parameter set considering the worst case of 0.69-inch AMOEL microdisplay panel: C=2.7 pF, I_{data}=270 pA, I_{max}=27 nA, V_{max}=250 mV, and ΔI=210 pA (1/2 LSB of 6-bit gray scale). Then, T_P=243 μsec, which is too large compared with the one scan time of 34.7 μsec at 60 tHz frame rate. Furthermore, it is very difficult to generating of very low-level current in the

current-mode data driver circuit. To solve the above two problems, the concept of de-amplifying current mirror pixel circuit technique can be applied.

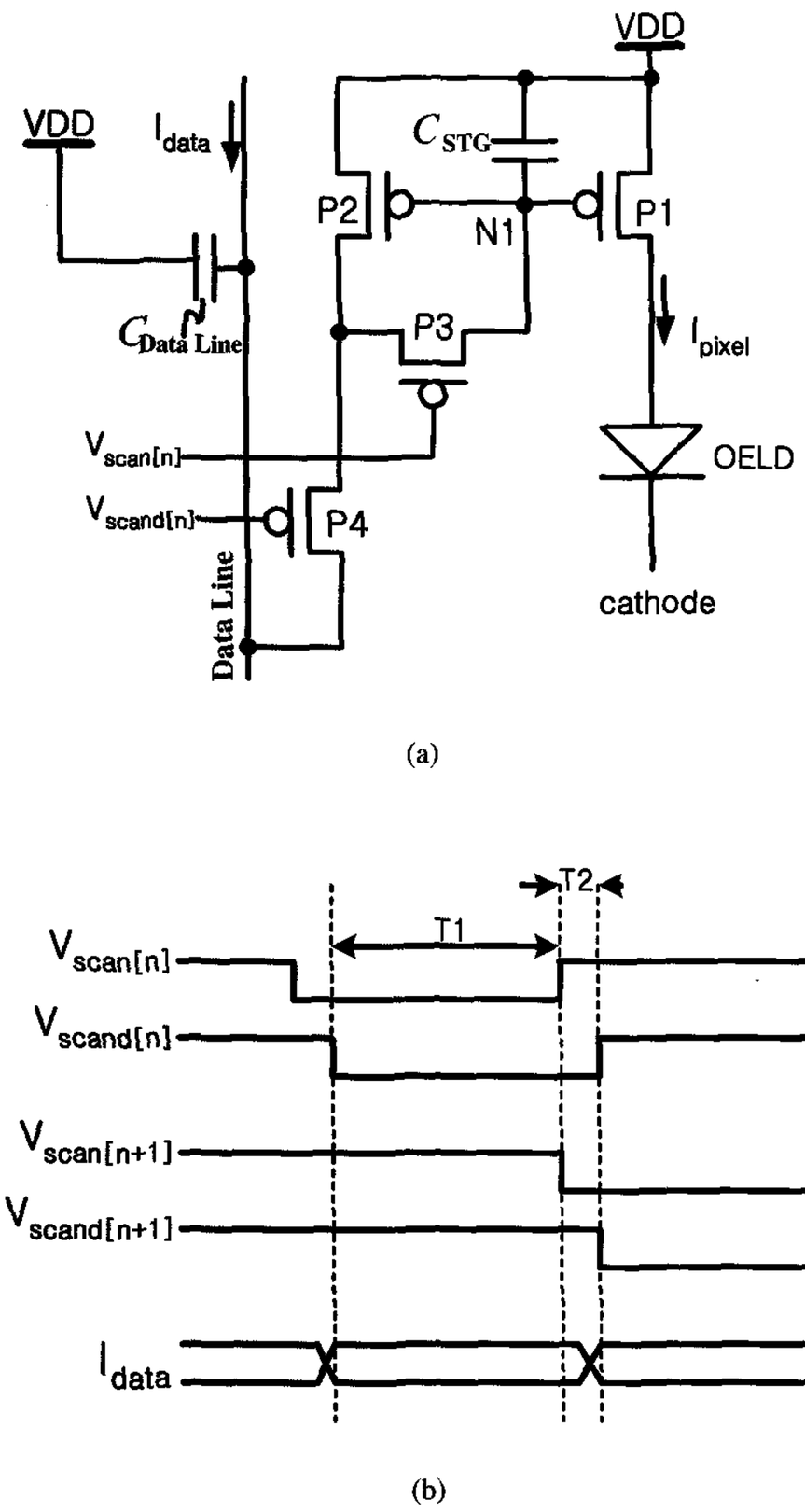

Fig. 6. (a) The schematic diagram of de-amplifying current mirror pixel circuit. (b) The timing relationship of three control lines ($V_{scan[n]}$, $V_{scand[n]}$, and I_{data}) of (a).

Fig. 6 (a) shows the schematic diagram of de-amplifying current mirror pixel circuit, which is composed of current mirror pair (P1 and P2), two switching transistors (P3 and P4), and one storage capacitance (C_{STG}). The anode electrode of OEL pixel is connected to the drain of driving transistor (P1). The pixel current I_{pixel} is determined by the node voltage at N1 in Fig. 6(a). And the I_{data} from current-mode data driver circuit determines the node voltage at N1 in Fig. 6(a). The P1 and P2 comprise of a current mirror pair. The current mirror ratio of P2 to P1 in Fig. 6(a) is much larger than 1. Fig. 6(a) has five external terminals (VDD, cathode, $V_{scan[n]}$, $V_{scand[n]}$, and data line) including three control lines ($V_{scan[n]}$, $V_{scand[n]}$, and data line). The two control lines of $V_{scan[n]}$ and $V_{scand[n]}$ originate from scan driver circuit as shown in Fig. 1. And the I_{data} comes from the current-mode data driver circuit. The timing relationship of three control lines ($V_{scan[n]}$, $V_{scand[n]}$, and I_{data}) is shown in Fig. 6(b). At T1 period, both $V_{scan[n]}$ and $V_{scand[n]}$ signals are low and P3 and P4 transistors in Fig. 6(a) are turned on. Then, P1 and the P2 transistors form a current mirror circuit. At this time, the I_{data} from current mode data driver circuit is programmed into P2 transistor. Then, the mirrored current I_{pixel} flows through the OELD pixel. The voltage at node N1 become fixed when the drain current of P2 equals I_{data}. At the end of T1, $V_{scan[n]}$ goes high and $V_{scand[n]}$ remains low. Then, P3 transistor is turned off while P4 transistor remains turned on. The voltage at node N1 in Fig. 6(a) is sampled and stored in the pixel storage capacitor of C_{STG}. At the end of T2, $V_{scand[n]}$ becomes high. The T2 timing difference between Vscan[n] and Vscand[n] is to reduce the sampling errors at node N1 in Fig. 6(a) by preventing P3 and P4 from simultaneously being turned off. Fig. 7 shows the SPICE circuit simulation results on the de-amplifying current-mirror pixel circuit as shown in Fig. 6(a). To show the circuit operations, the input data current (I_{data}) pulses in Fig. 7(a) are applied to the data line in Fig. 6(a). The time durations of T3 and T4 in Fig. 7(a) are 35 μsec and 150 μsec, respectively. Figs. 7(b) and (c) show the simulated pixel current (I_{pixel}) when T2 as shown in Fig. 6(b) is zero and not, respectively. The large sampling error without T2 period is shown in Fig. 7(b). From Fig. 7(c), it can be seen that there still exist sampling errors, but they are much less than those shown in of the Fig. 7(b). Fig. 7(d) shows the correlation between the sampled pixel data current (I_{pixel}) and input data current (I_{data}). From Fig. 7(d), it can be known that the sampled pixel data current has a linear relationship with the input data current even when there are sampling errors. This(in turn) means that it does not need any γ-correction in the current-mode data driver circuit. This will be mentioned again in Section 3.

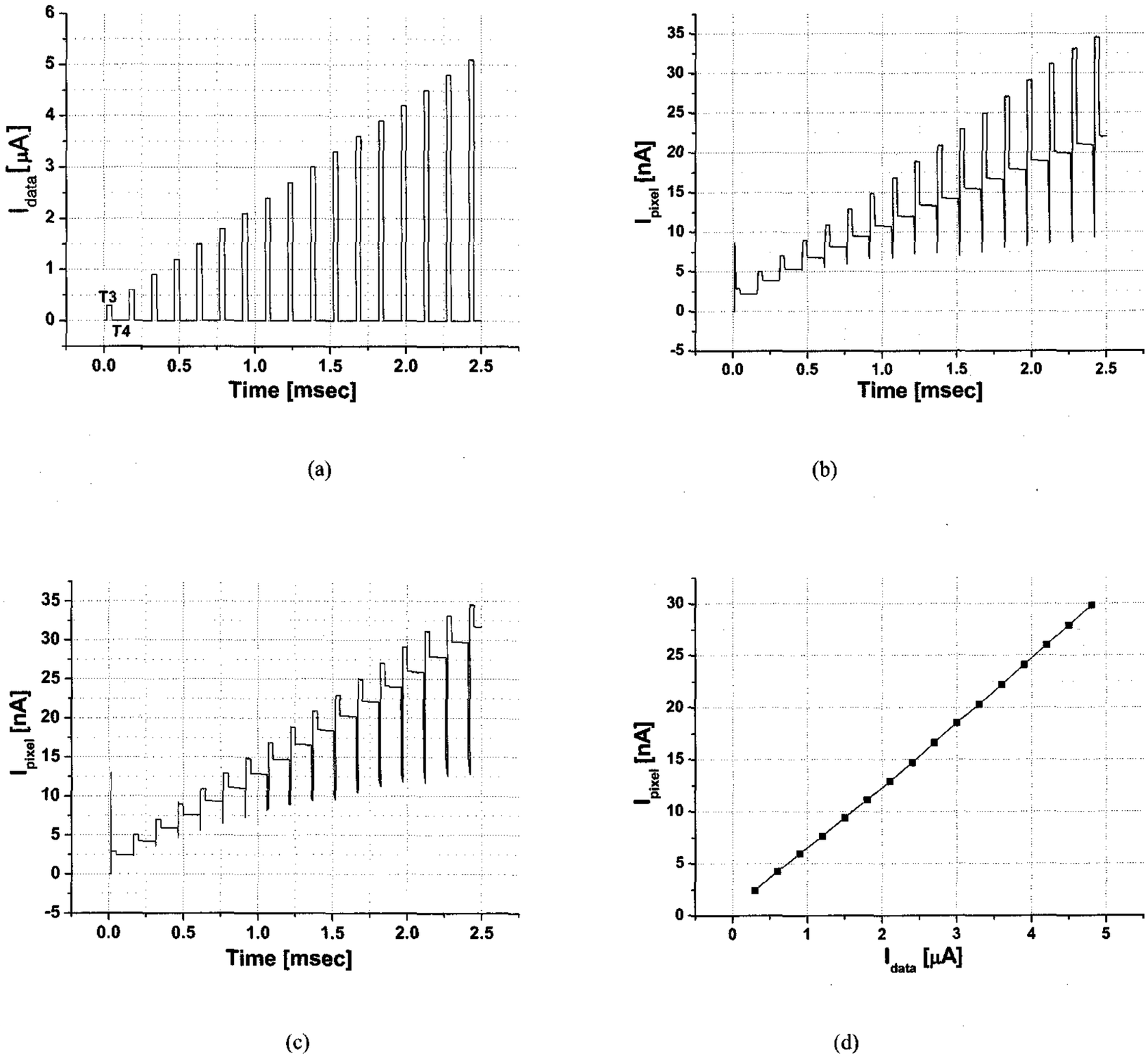

Fig. 7. SPICE simulation results on the de-amplifying current mirror pixel circuit as shown in Fig. 6(a) · (a) The input current pulses (I_{data}); (b) The output pixel current waveforms (I_{pixel}) when T2=0 sec in Fig. 6(a); (c) The output pixel current waveforms (I_{pixel}) when T2>0 sec in Fig. 6(a); and (d) The linear relationship of I_{pixel} versus I_{data}.

3. Current-Mode Data Driver Circuit with Threshold Voltage Compensation

As shown in Fig. 1, the proposed current-mode data driver circuit is composed of the shift register block with 852 stage, the digital video data sample and hold block, and the binary-weighted 6-bit current-mode DACs block. The binary-weighted 6-bit current-mode DAC generates 64-gray current levels. Because the current programmable pixel circuit is programmed using the data driver circuit having the advantages of threshold voltage and mobility compensation, the display uniformity of silicon-based AMOEL microdisplay, as shown in Fig. 1, is greatly dependent on the channel-to-channel uniformity of the 6-bit current-mode DACs as described in the introduction. And the mobilities across the silicon wafer are assumed to be the same. So, the main cause for the non-uniform channel-to-channel current outputs is the difference in the threshold voltages of the wide spreading current-mode DACs. S. Y. Chin and C. Y. Wu have proposed a concept of threshold voltage compensation by using the two matched transistors as shown in Fig. 8 [9]. But this circuit has two problems to be applied directly in the current-mode data driver circuit in this paper. That is, the output current is susceptible to the ground bouncing. If the width and the length of ground metal line are 100 μm and 15500 μm, respectively, then the calculated ground line resistance would be 12.4 Ω, where the sheet resistance of ground metal is 0.08 Ω/□. If we use the external two pads which

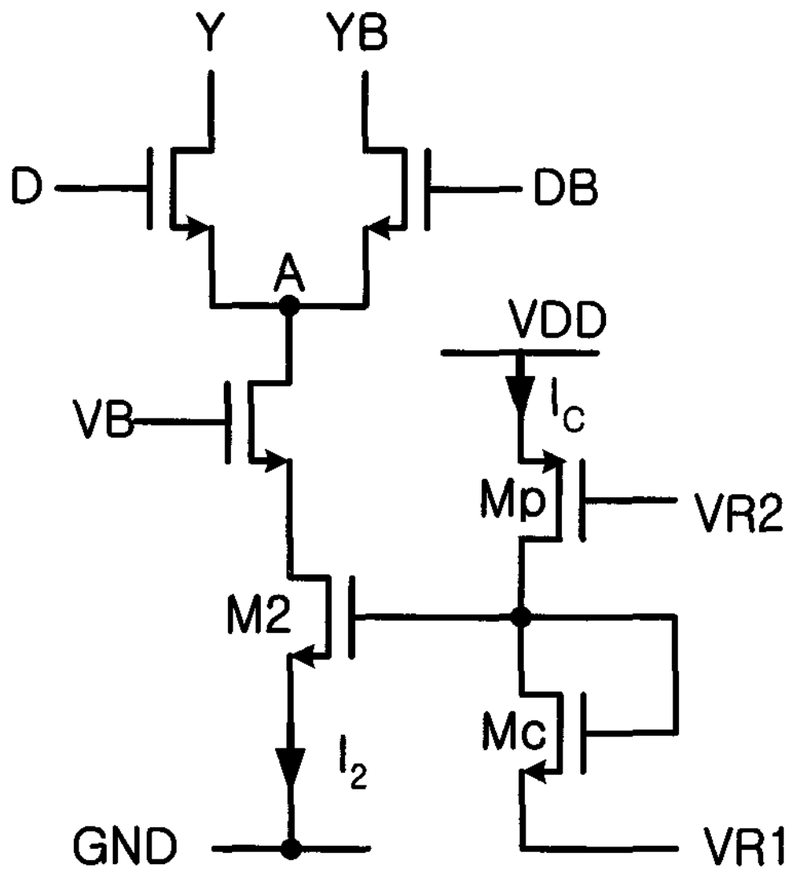

Fig. 8. The current source with threshold voltage compensation [9].

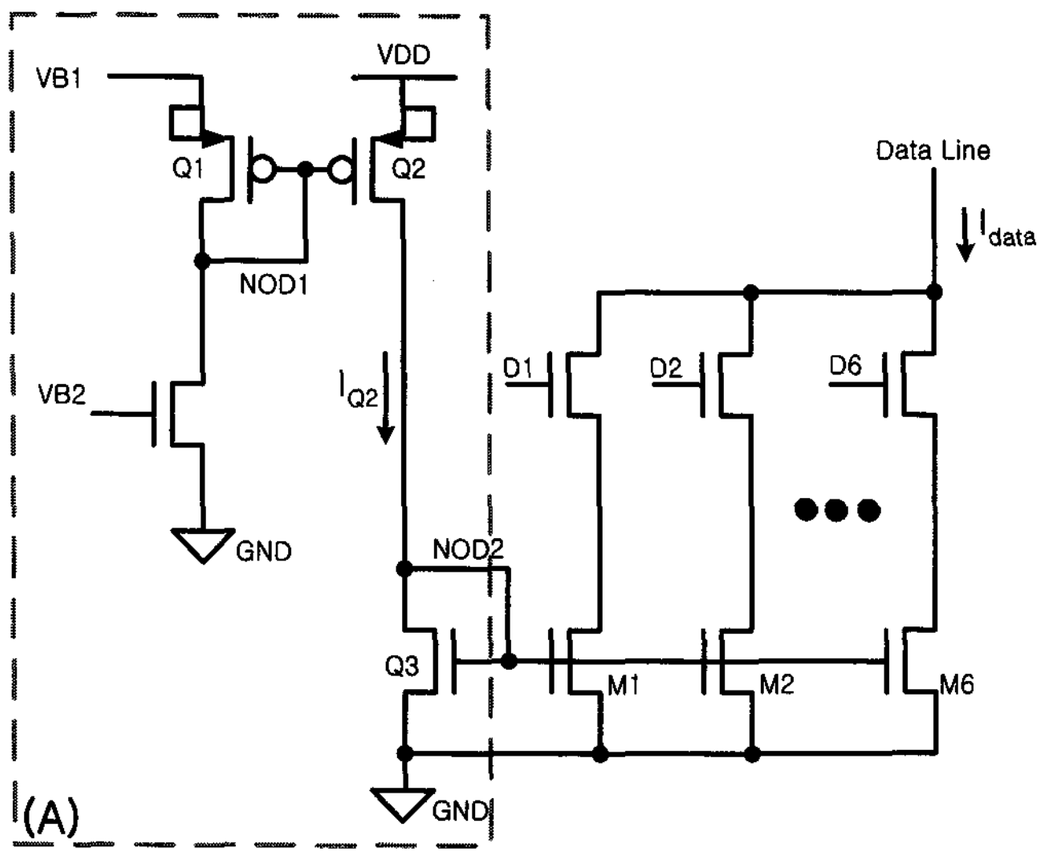

Fig. 9. The current-mode 6-bit DAC circuit that has threshold voltage compensation circuit block (A).

are connected to both ends of the ground line, the maximum effective resistance would be the center point of the ground line from one of the ground pads, which is calculated by 6.2 Ω. So, at each line addressing time (≈34.7 μsec at 60 Hz), if the total data current, which is sums to be about 11mA at full white level, flow through the ground line, the voltage difference between the center point and the end point of the ground line will be about 68 mV. SPICE simulation result gives about 50 % current variation. Furthermore, the circuit of Fig. 8 occupies a large layout area due to the threshold voltage compensation for every-bit current sources.

Fig. 9 shows the proposed current-mode 6-bit DAC circuit with threshold voltage compensation. The reference current I_{Q2} for one channel 6-bit current-mode DAC is generated according to the V_{B1} from the circuit block (A) in Fig. 9. The transistors Q1 and Q2 are assumed to have the same widths and lengths. And they are very close in layout. Then, the reference current I_{Q2} is given by the following equation (6).

$$\left|I_{Q1}\right| = K(V_{B1} - V_X - \left|V_{th1}\right|)^2 \tag{2}$$

$$V_X = V_{B1} - |V_{th1}| - \frac{1}{\sqrt{K}}\sqrt{|I_{Q1}|} \quad (3)$$

$$|I_{Q2}| = K(V_{DD} - V_X - |V_{th2}|)^2 \quad (4)$$

$$= K(V_{DD} - V_{B1} + |V_{th1}| + \frac{1}{\sqrt{K}}\sqrt{|I_{Q1}|} - |V_{th2}|)^2 \quad (5)$$

$$\approx K(V_{DD} - V_{B1} + |V_{th1}| - |V_{th2}|)^2 \quad (6)$$

In detail, the channel current, I_{Q1} of transistor Q1 can be expressed by (2), where K equals $\mu_p C_{ox}(W/L)$ and V_x is the node voltage at NOD1 in Fig. 9. And the reference current, I_{Q2} is determined by (5). If we set the current I_{Q1} to be very low by setting V_{B2} close to the ground voltage, then $\frac{1}{\sqrt{K}}\sqrt{|I_{Q1}|}$ shall be negligible due to $I_{Q1} << I_{Q2}$. Finally, the reference current I_{Q2} is determined by (6). In (6), it is known that I_{Q2} does not depend on the V_{th2} alone but depends on the threshold voltage difference between two transistors (Q1, Q2) of $|Vth_2|-|Vth_1|$. This means that, if two transistors are locally matched, which in turn means they have the same widths and lengths and are very close in layout, the undesirable current variation of the current sources can be significantly reduced.

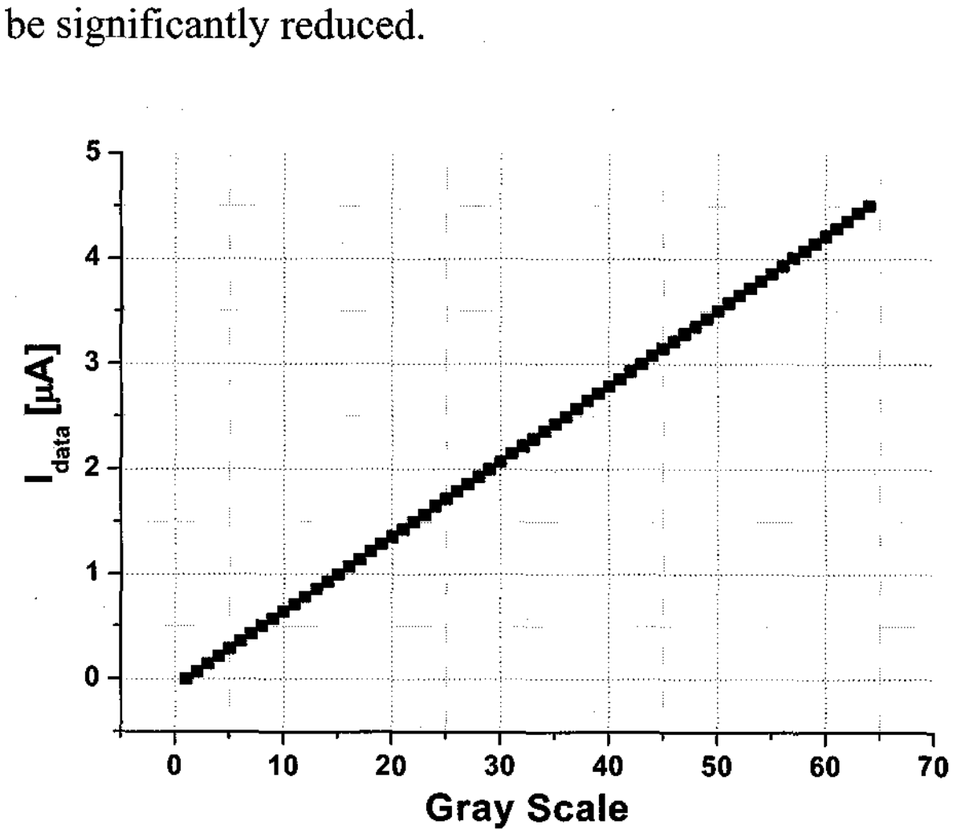

Fig. 10. PICE simulation results of I_{data} in Fig. 9 according to the 64-gray scale, which shows high linearity.

Additionally, the proposed current-mode 6-bit DAC has immunity to the ground bouncing effect, because the I_{out} is the summation of mirror currents of I_{Q2}. And the VDD bouncing problem can also be negligible due to the small I_{Q2}, whose value is set as the same current level of least significant bit of the current-mode 6-bit DAC. The voltage at NOD2 as shown in Fig. 9 varies with the voltage variation on the ground line. So, the gate-to-source voltage of current source remains the same regardless of the ground bouncing. The width ratios of Q3 to M1, M2, M3, M4, M5, and M6 are 1, 2, 4, 8, 16, 32, respectively. And D1, D2, D3, D4, D5, and D6, as shown in Fig. 9, are switching transistors that determine the output current level I_{out} according to the combination of input 6-bit digital data. And because they are very close in layout the mismatch problem among M1, M2, M3, M4, M5, and M6 transistors can be minimized, Fig. 10 shows the simulation results of I_{data} according to the gray scales. From Fig. 10 and Fig. 7(d), it can be known that it

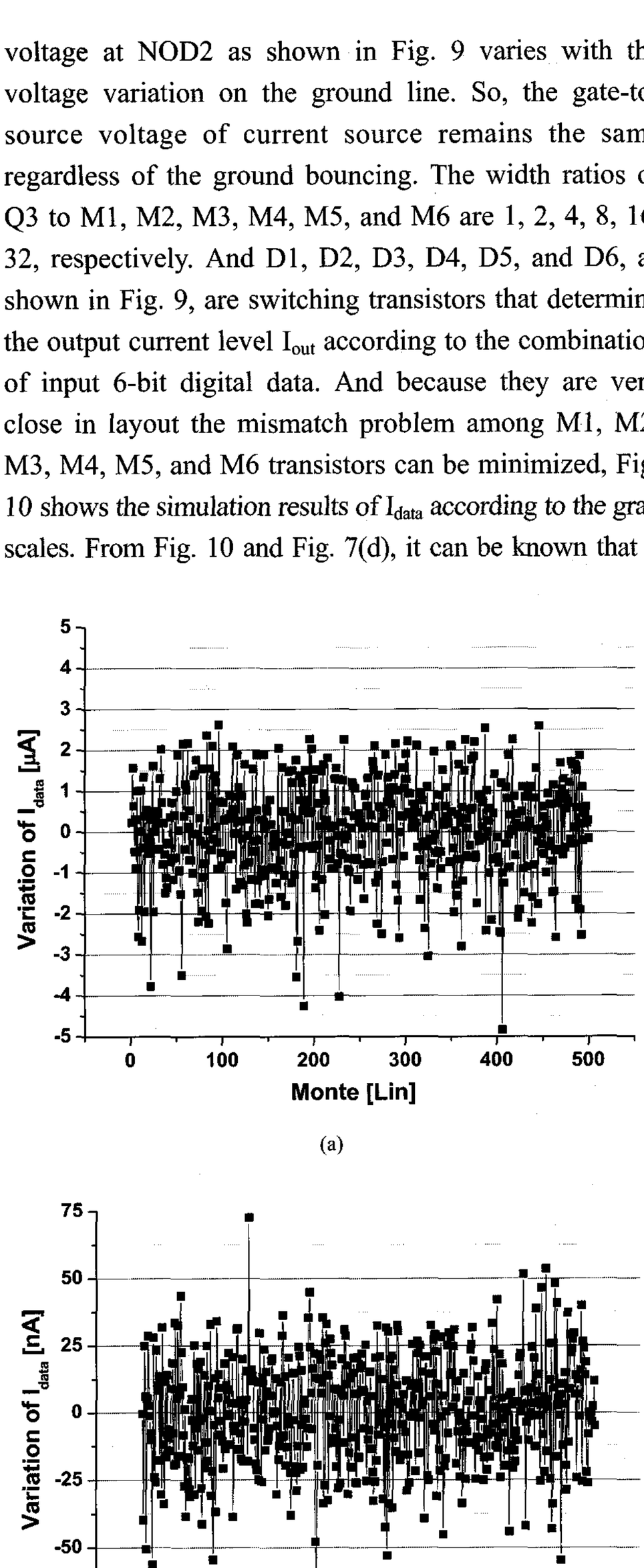

Fig. 11. Monte-Carlo simulation results for (a) the conventional weighted current sources that have no threshold voltage compensation block (A) in Fig. 9 and (b) the current sources with the proposed threshold-voltage compensation block (A) in Fig. 9.

does not need γ-correction in the proposed current-mode data driver circuit. SPICE Monte-Carlo simulation results for both current-mode 6-bit DAC without threshold voltage compensation circuit and current-mode 6-bit DAC with threshold voltage compensation circuit (A), as shown in Fig. 9, are shown in Figs. 11(a) and (b) at peak luminance, respectively. Fig. 11 shows that the proposed current-mode 6-bit DAC with the threshold voltage compensation circuit can reduce channel-to-channel current variation from ±2.5 μA to ±45 nA assuming that the threshold voltage variations of both NMOS and PMOS devices are within ±70 mV with Gaussian distribution. The deviation of ±45 nA in Fig. 11(b) results in ±0.6 LSB gray scale deviation. This means that the designed 0.69-inch AMOEL microdisplay has very uniform display view. The summary of designed silicon-based 0.69-inch AMOEL microdisplay panel is shown in Table 1.

Table 1. Summary of silicon-based 0.69-inch AMOEL microdisplay panel

Chip Size	18.4×12.3 mm^2
Display Area	0.69-inch diagonal
Resolution	852 (×RGB)×480
Pixel Size	18×18 μm^2
Luminance	150 cd/m^2 (Max)
Sub-Pixel Current (RGB each)	27 nA (Max)
Contrast Ratio	100:1
Power Consumption	300 mW (Max)
Gray Scale	64-gray
Technology	0.35 μm CMOS with CMP process
Supply Voltages	VDD=4.5 V, $V_{cathode}$=-4.6 V

4. Conclusions

In this paper, we presented the circuit design and the analysis of silicon-based 0.69-inch AMOEL microdisplay with integrated driver circuits. The de-amplifying current mirror pixel circuit technique is proven to be also effective for small size display by reducing the pixel data programming time. And it also helps to design the current-mode data driver circuit, easily. The current-mode data driver circuit with threshold voltage compensation can obtain less than ±0.6 LSB channel-to-channel variation under ±70 mV threshold voltage variations of both NMOS and PMOS transistors. As a result, we can obtain very uniform AMOEL microdisplay panel by using the proposed de-amplifying current-mirror pixel circuit and the current-mode data driver circuit with threshold voltage compensation.

Acknowledgement

The authors thank Hak-Su Kim and Sung-Tae Kim of LG Electronics in Korea for their help and support, Dr. O.Prache of eMagin Co. in the USA for supplying the measured I-V data of OEL pixel, and lastly, Byong-Chan Lim of Hanyang University for his support in designing the LVDS interface circuitry.

References

[1] R. M. A. Dawson, Z. Shen, D. A. Furst, S. Connor, J. Hsu, M. G. Kane, R. G. Stewart, A. Ipri, C. N. King, P. J. Green, R. T. Flegal, S. Pearson, W. A. Barrow, E. Dickey, K. Ping, C. W. Tang, S. Van Slyke, F. Chen, J. Shi, J. C. Sturm, and M. H. Lu, in SID Tech. Dig. (1998), p. 11.

[2] Y. He, R. Hattori, and J. Kanicki, IEEE Trans. Electron Devices, **48**, 1322 (2001).

[3] R. M. A. Dawson, Z. Shen, D. A. Furst, S. Connor, J. Hsu, M. G. Kane, R. G. Stewart, A. Ipri, C. N. King, P. J. Green, R. T. Flegal, S. Pearson, W. A. Barrow, E. Dickey, K. Ping, S. Robinson, C. W. Tang, S. Van Slyke, F. Chen, J. Shi, M. H. Lu, and J. C. Sturm, in IEDM Tech. Dig. (1998), p. 875.

[4] M. T. Johnson, I. M. Hunter, N. D. Young, I. G. J. Camps, H. Lifka, and A. J. M. v. d. Biggelaar, in IDW Tech. Dig. (2000), p. 235.

[5] S. J. Bae, H. S. Lee, J. Y. Lee, J. Y. Park, and C. W. Han, in SID Tech. Dig. (2000), p. 358.

[6] A. Yumoto, M. Asano, H. Hasegawa, and M. Sekiya, in AD and IDW Tech. Dig. (2001), p 1395.

[7] Y. S. Na, O. K. Kwon, and H. S. Kim, Korean Patent No. 10-0327374.

[8] O. Prache, in SID Tech. Dig. (2001), p. 514.

[9] S. Y. Chin and C. Y. Wu, IEEE Trans. JSSC, **29**, 1374 (1994).